ELSEVIER

Thermochimica Acta 390 (2002) 169–177

thermochimica acta

www.elsevier.com/locate/tca

Thermal decomposition study of the coordination compound $[Fe(urea)_6](NO_3)_3$

O. Carp[a,*], L. Patron[a], L. Diamandescu[b], A. Reller[c]

[a]*Institute of Physical Chemistry "I.G. Murgulescu", Spl. Independentei no. 202, Sect. 6, Bucharest, Romania*
[b]*Institute of Atomic Physics, National Institute for Materials Physics, P.O. Box MG-7, R-76900 Bucharest, Romania*
[c]*Solid State Chemistry, University of Augsburg, Universitätstrasse 1, D-86159 Augsburg, Germany*

Received 13 October 2001; received in revised form 13 February 2002; accepted 24 February 2002

Abstract

The thermochemical behavior of the coordination compound $[Fe(urea)_6](NO_3)_3$ was studied by simultaneous CG–TG–DTG–DTA and mass spectrometry methods non-isothermal conditions. The compound decomposes at ~200 °C into a mixture of spinel-type oxides and hematite. The nature and particle size of the final decomposition products are strongly associated with the conditions during the thermal treatments, in particular the heating rate and the calcination temperature. A certain fraction of the products are formed as nanometric particles; they show superparamagnetic behavior at room temperature. The comparably low temperature of the calcination treatments of this compound is a promising perspective to attain small sized magnetic powders.

Keywords: Iron–urea coordination compound; Thermoreactivity; Iron oxides

1. Introduction

In the last few decades, different methods have been applied to obtain iron oxide powders for various applications. The aim of the endeavor was not only to obtain the requested powder properties but also to make use of less energy intensive and more environmentally friendly procedures.

Magnetite, maghemite and hematite represent—besides their uses as inorganic pigments, catalysts or magnetic recording media—raw materials for synthesis of iron containing mixed oxides of ferritic type (specially with cubic and hexagonal structure). The preparation method determines the final powder characteristics, like shape, specific surface and porosity that are of great importance in the subsequent processing for specific applications. The synthesis of these oxide materials is quite complicated and lengthy. Iron oxides are generally prepared by co-precipitation of hydroxide [1–4] and carbonate [5], sol–gel [6], hydrothermal technique [7–12] and by thermal decomposition of some simple iron salts such as oxalates [13,14], citrate [15] and coordination compounds containing hydrazine [16].

This work is aimed at showing the thermal behavior (in air or inert atmospheres) of the coordination compound $[Fe(urea)_6](NO_3)_3$. Thermal decomposition of this compound represent a new possible way to synthesize some iron oxides. From the theoretical point of view, the interest is focused on the mechanistic course of the thermal transformation. From the practical perspective, the aim of investigation is to explore the possibilities of using some coordination

* Corresponding author. Fax: +40-1-650-7615.
E-mail address: carp@apia.ro (O. Carp).

0040-6031/02/$ – see front matter
PII: S0040-6031(02)00085-0

compounds containing the urea ligand and nitrate anion as outer sphere ion as precursors to nanosized oxides. Due to the presence of the reducing groups (urea) in the coordination sphere and of vigorous oxidizing group (NO_3^-) in the ionization sphere, fine particles oxides are formed. Because the dissociation occurs at low temperatures with a large amount of gas evolving in a highly exothermic manner this approach represents a new route in the synthesis of some iron oxides.

2. Experimental

The coordination compound was separated by means of two synthesis methods, a solid state phase reaction method and a co-precipitation process. Details about the synthesis method are present elsewhere [17]. Both synthesis methods lead to the same pale-green iron compound of the molecular formula $[Fe(urea)_6](NO_3)_3$. The total metal content was determined by atomic adsorption spectroscopy, and the carbon and hydrogen content by using a combustion method coupled with a chromatrographic technique. The iron content (Fe_{total} and Fe^{2+}) of some intermediates were determined by titration with standard potassium bichromate solution [18]. Anal. found (calcd): Fe: 9.07 (9.27); C: 12.05 (11.96); N: 34.42 (34.89); H 3.71 (3.98).

Structural investigations of powder samples have been carried out using a Philips PW 1049 diffractometer at a scanning rate of 1° ($=2\theta$)/min using Co Kα radiation. The UV–Vis reflectance spectra were recorded with a spectrophotometer in the range of 11000–54000 cm^{-1}. The IR spectra were recorded with a BIORAD FT-IR 1255 type spectrometer.

Mössbauer spectra were obtained at room temperature with a constant acceleration spectrometer (PROMEDA type equipment) using a 10 mCi Co^{57} (Rh) source. The spectra were least square fitted assuming Lorentzian line shape. The TEM investigations were performed on a JEM 200 CX microscope.

The magnetic susceptibilities of the initial coordination compound and decomposition intermediates were measured on a Faraday balance at room temperature. The complex $Hg[Co(SCN)_4]$ was used for calibration. For the paramagnetic compound (coordination compound) the magnetic moment in Bohr magneton was calculated from

$$\mu_{(MB)} = 2.8282(T\chi_{mol})^{1/2} \quad (1)$$

where χ_{mol} represents the molar susceptibility and T the absolute temperature.

The thermal decomposition of the title compound $[Fe(urea)_6](NO_3)_2$ has been recorded with a simultaneous thermogravimetry/mass spectrometry unit made by a NETZSCH STA 4009 coupled with a capillary to a BALZERS QMS 421 mass spectrometer. Thermochemical investigations were carried out under dynamic conditions in air and argon, with sample mass about 20 mg at heating rates of 2 K/min. The DSC investigations and thermomicroscopy were performed on a Mettler TA 2000 thermobalance and Mettler FP 84 thermomicroscope.

3. Results

3.1. Physico-chemical characterization of the coordination compound

The recorded IR spectrum compared with that of urea (Fig. 1) indicates that the metal ion is coordinated to urea through oxygen atoms. This coordination mode leads to a decrease of the CO stretching frequencies and an increase in the CN stretching ones [19–23]. Bands assigned to the vibration mode of NO_3^- anion are also identified.

In the electronic spectrum bands characteristic for Fe(III) ions in an octahedral environment (Fig. 2) are observed. The weak detected band intensities and pale-green color of the compound are due to the spin and parity forbidden nature of the ligand field transitions of high spin Fe(III) d^5.

The magnetic measurements confirm the existence of high spin Fe(III) since the magnetic moment (6.10 BM) is close to the spin only-value for high spin Fe(III) (5.92 BM) [24].

3.2. Thermal behavior and reactions stoichiometries

The thermal decomposition of the investigated compound is complicated due to the presence of both reducing and oxidizing agents (urea and nitrate ions) in the coordination compound entity and by the formation of iron hydroxides, oxyhydroxides and oxides

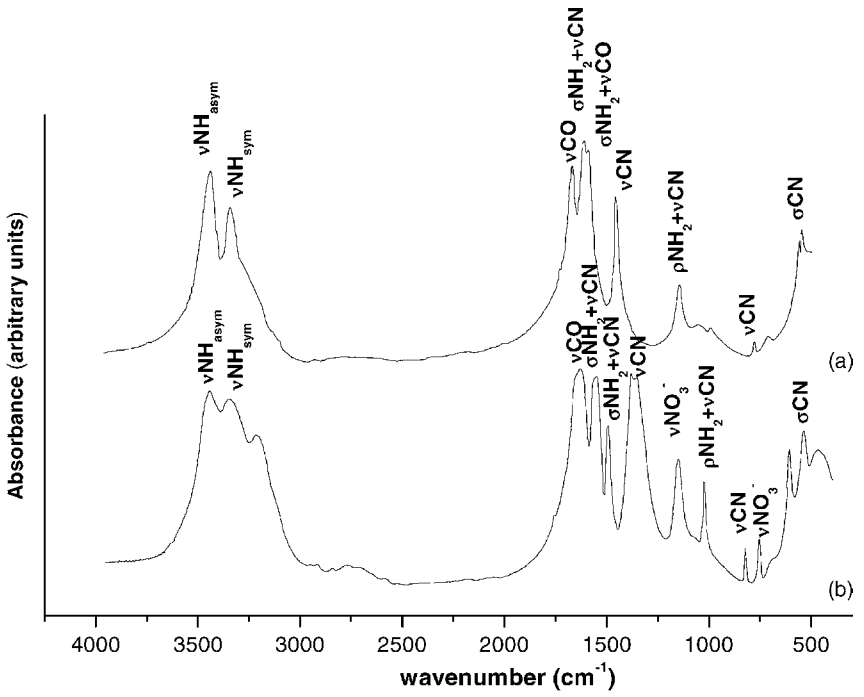

Fig. 1. IR spectra of (a) urea and (b) $[Fe(urea)_6](NO_3)_3$.

species upon heating. The progress of the degradation is practically not affected by the type of atmosphere. The TG, DTG and DTA data obtained on heating in air are shown in Fig. 3. The temperature variation of the major species formed as seen by MS is shown in Fig. 4. The experimental total mass loss recorded by TG measurements is 83.9/83.7% (argon/air) in comparison with the theoretical value of 83.29% when the solid residue is assumed to be α-Fe_2O_3.

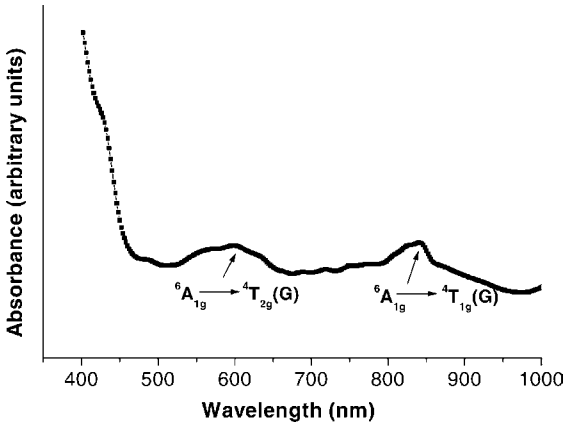

Fig. 2. Electronic spectrum of $[Fe(urea)_6](NO_3)_3$.

The decomposition reaction takes place in three stages in the temperature range 155–250 °C. The decomposition starts 15 °C below the melting point, with a fast and strong exothermic process, characterized by a weight loss of ~75%, assigned to a simultaneously release of urea and decomposition of nitrate ion. The decomposition products are identified as: H_2, H_2O, CO_2 and NH_3, N_2, NO_2 and HNCO. It is followed by two decomposition steps, with a total weight loss of ~9%, the first is associated with an endothermal heat effect, the second with an exothermal one. In both these processes water is release. In addition were traces of CO_2 identified. The behavior may be explained as follows: during the first reaction step a highly reactive solid residue forms in the presence of water, which is generated during the redox reaction of the NH_3/NO_3^- system. In the solid residue the Fe^{3+} ions are partially reduced to Fe^{2+}, i.e. iron hydroxides and oxyhydroxides species are obtained. Upon heating further water removal takes place. The overall exothermal effect associated with the third

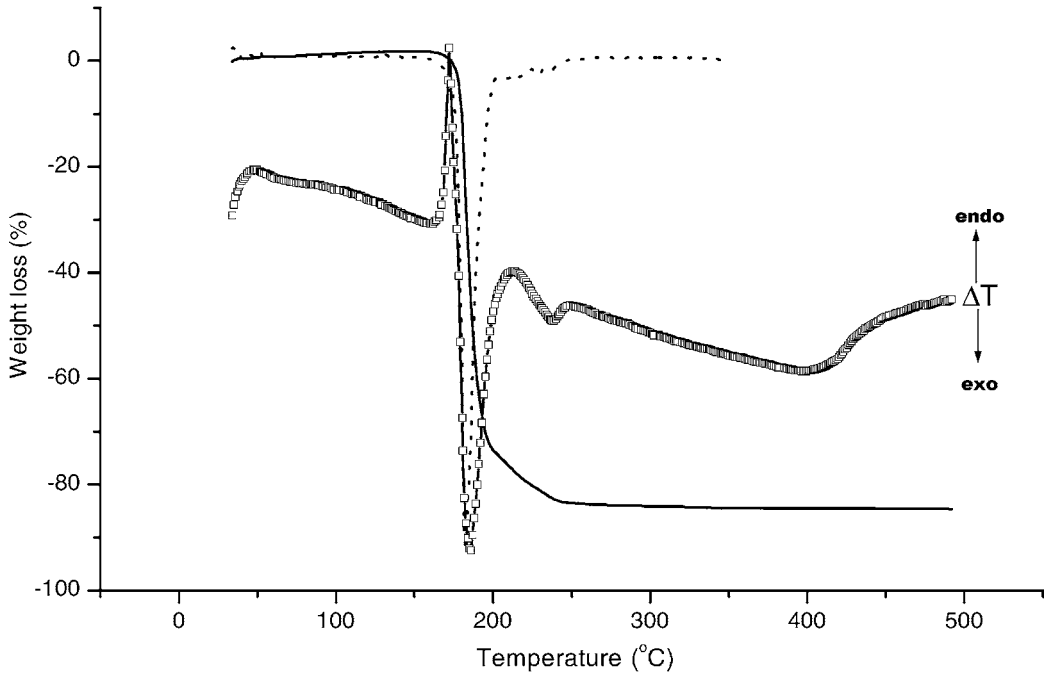

Fig. 3. TG (—), DTG (- - -) and DTA (–□–□–) curves of $[Fe(urea)_6](NO_3)_3$ (air heating rate: 1.5 °C/min).

decomposition is due to a crystallization process, which occurs simultaneously with the dehydration stage. At ∼430 °C the DTA curve reveals a phase transformation assigned to the known γ-$Fe_2O_3 \rightarrow \alpha$-$Fe_2O_3$ phase transition. All these decomposition and phase transition steps are accompanied by color changes of the solids involved in the following sequence:

$$\text{pale-green} \overset{\sim 155-180\,^{\circ}C}{\rightarrow} \text{dark brown} \overset{\sim 180-190\,^{\circ}C}{\rightarrow} \text{bluish-green} \overset{\sim 190-205\,^{\circ}C}{\rightarrow} \text{black} \overset{\sim 430\,^{\circ}C}{\rightarrow} \text{red}$$

Table 1 shows the relative amount of the evolved decomposition products (semiquantitative results obtained from MS measurements).

3.3. Characterization of the final products

The solid decomposition products consist of a mixture of spinel-type oxides (magnetite and γ-Fe_2O_3) and α-Fe_2O_3. This conclusion is reached by the presence of the characteristic vibration and transition frequencies (Fig. 5a–c), and by the superposition of magnetic sextets and doublets in the Mössbauer spectra (Fig. 6a and b), which correspond to different iron oxides phases. The best fit of the Mössbauer spectra was obtained by taking in to account two magnetic hyperfine sextets together with two quadrupolar doublets. The Mössbauer parameters given by the computer fit (hyperfine magnetic field H, isomer shift IS and quadrupole splitting QS as well as the relative area of subspectra) are presented in Table 2. The presence of the magnetic oxides is established

Table 1
Relative amount of the evolved gaseous products

Product	Atmosphere	
	Nitrogen	Air
H_2	4	2
$m/z = 16$	32	22
NH_3	30	25
H_2O	10	11
N_2	9	22
NO	3	2
O_2	0	3
HNCO	2	1
$CO_2(N_2O)$	15	18
NO_2	Traces	Traces

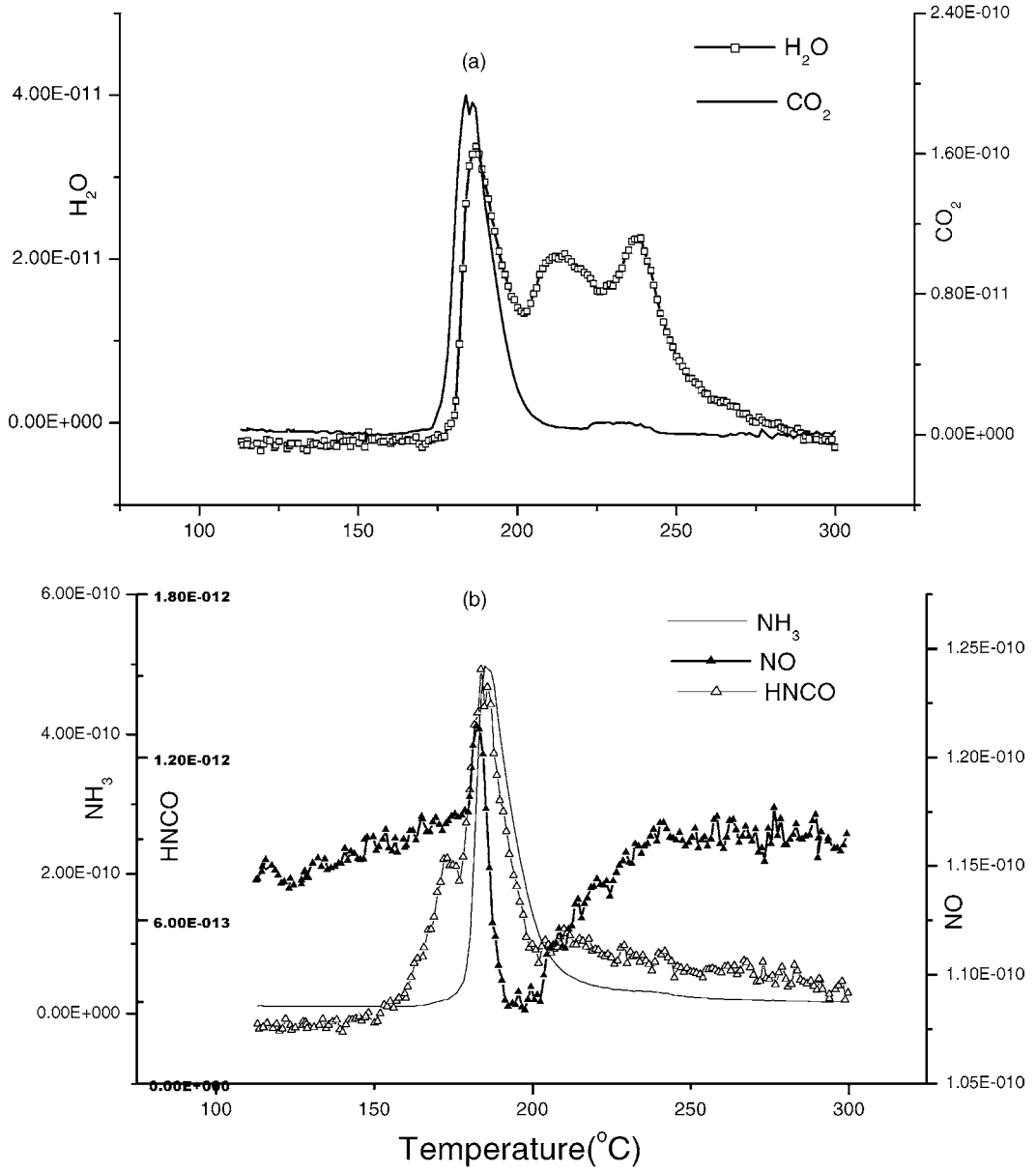

Fig. 4. Ion intensities curves of $[Fe(urea)_6](NO_3)_3$ (air heating rate: 1.5 °C/min).

also by the saturation magnetization values obtained (Fig. 7).

During the reaction progress, green rust (II) may be formed. This affirmation is supported by the presence of Fe^{2+} in the intermediate solid, the bluish-green color detected by thermomicroscopic investigations and the release of traces of CO_2 in the same temperature range. The infrared spectra indicates the presence in the temperature range 200–300 °C—besides the bands assigned to the inverse-type spinels (high-frequency band assigned the tetrahedral sites and a low one ascribed to the octahedral sites [25,26]), bands were assigned to the iron oxide α-Fe_2O_3 [26]. The band of $\sim$19,000 cm^{-1} is unambiguously assigned to a

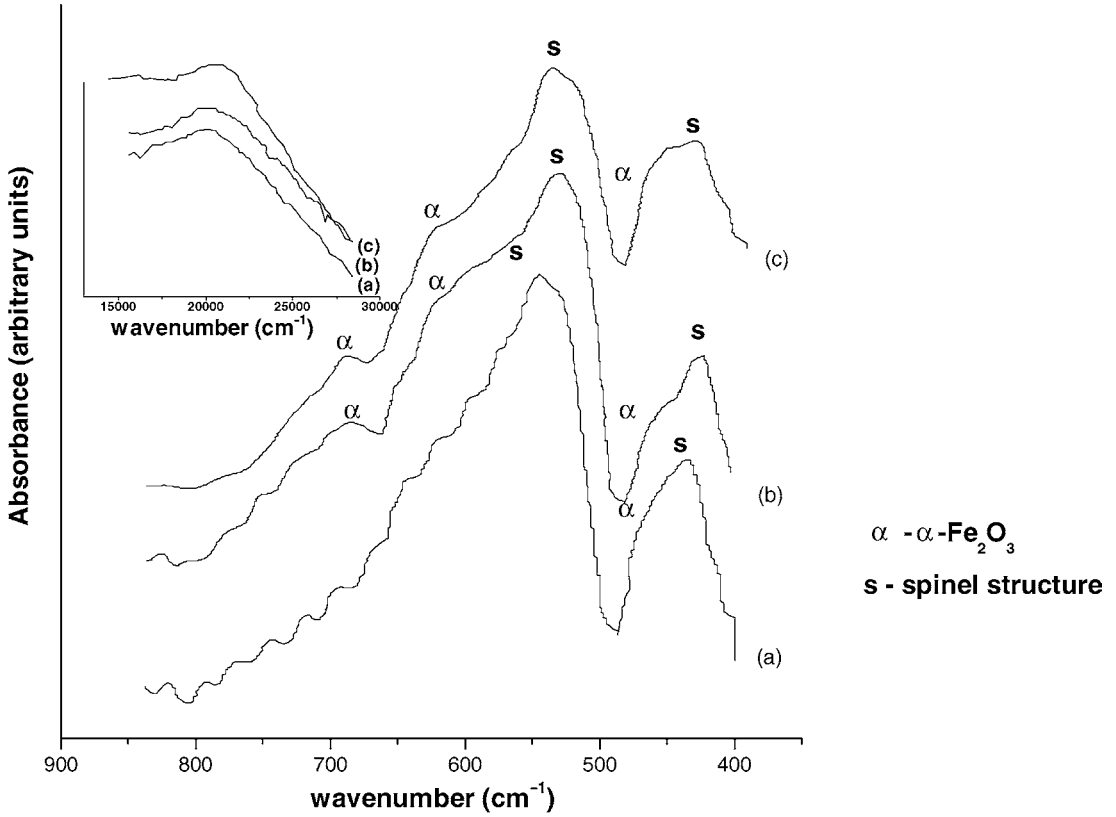

Fig. 5. IR and UV–Vis of the oxidic product: (a) $T = 200\,^{\circ}C$, time: 4 h, heating rate: 1.5°/min; (b) $T = 200\,^{\circ}C$, time: 4 h, heating rate: 3°/min; (c) $T = 300\,^{\circ}C$, time: 4 h, heating rate: 3°/min.

Table 2
Mössbauer fit parameters of the oxides obtained at 200 °C

Mössbauer pattern	IS[a] (mm/s)	QS[b] (mm/s)	H^c (kOe)	Relative areas (%)	Site assignment
Heating rate: 1.5 °C/min, calcination time: 4 h					
Sextet	0.35	−0.02	523	52.3	α-Fe_2O_3
Sextet	0.59	0.03	472	13.7	Fe_3O_4
Doublet	0.29	0.98	–	20.2	Superpara
Doublet	0.29	0.59	–	13.8	Superpara
Heating rate: 3 °C/min, calcination time: 4 h					
Sextet	0.36	−0.02	524	68.6	α-Fe_2O_3
Sextet	0.27	0.10	508	13.4	γ-Fe_2O_3
Doublet	0.23	0.86	–	14.6	Superpara
Doublet	0.23	0.49	–	3.4	Superpara
Errors	±0.01	±0.02	±1	±0.8	

[a] Isomer shift. The values are relative to α-iron.
[b] Quadrupole splitting.
[c] Hyperfine magnetic field.

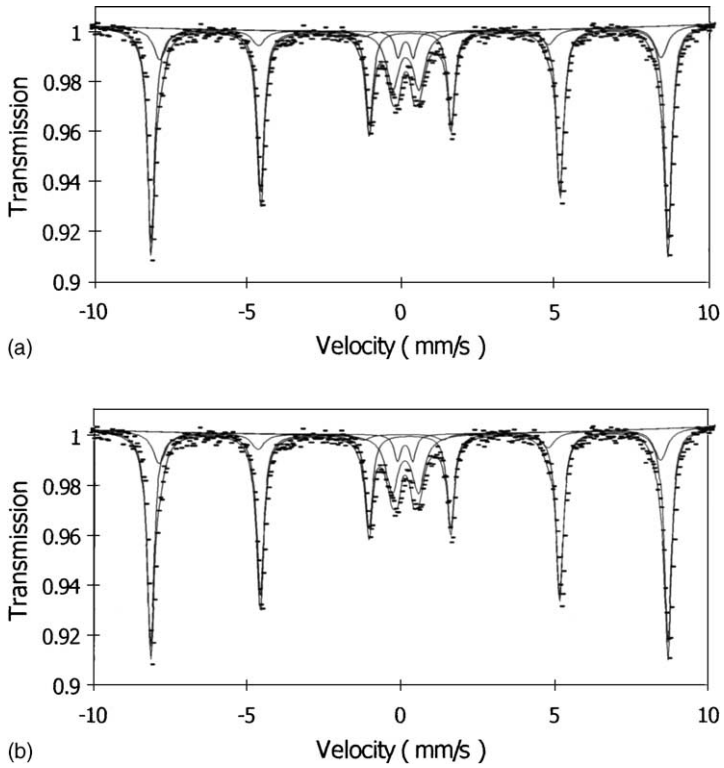

Fig. 6. Mössbauer spectra of the oxides obtained at 200 °C.

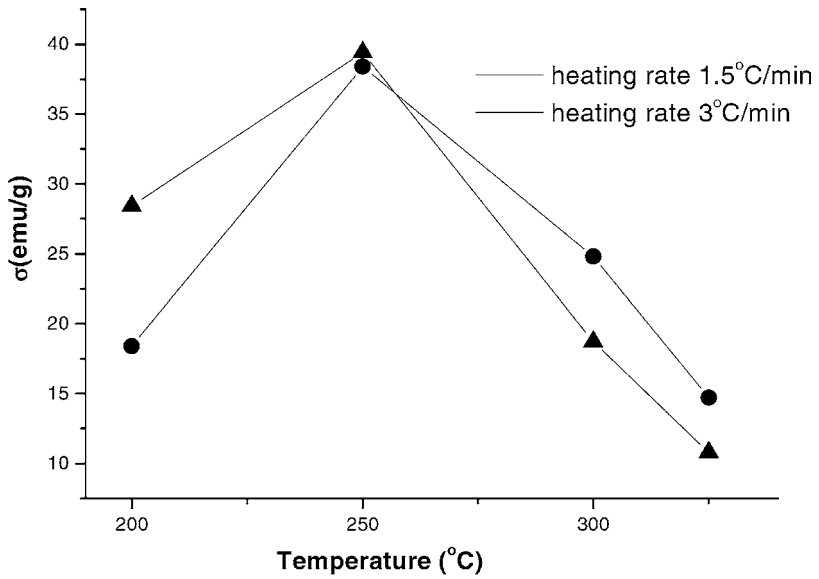

Fig. 7. Evolution of the saturation magnetization with the calcination conditions (calcination time 4 h).

composite of $^6A_1 \rightarrow {}^4T_{2g}({}^4G)$ ligand field transition of tetrahedral Fe(III) and $^6A_1 + {}^6A_1 \rightarrow {}^4T_{2g} + {}^4T_{2g}({}^4G)$ pair transitions [27]. The bulk spinel-type oxide detected at 175 and 200 °C (heating rate: 1.5°/min) is probable Fe_3O_4 (see Table 2). A rather low Mössbauer effect (the second sextet in Fig. 7) accompanied by a very large line width, reveals a poorly crystallized phase and an incompletely formed bulk phase accompanied by a nanoscopic by-product. These findings are also confirmed by the TEM investigations.

The population of nanoparticles with superparamagnetic behavior (central doublets in Mössbauer spectra) decreases when increasing the heating rate and calcination temperature. The values of the hyperfine parameters imply Fe^{3+} ions. In the presence of superparamagnetic effects the phase assignment from Mössbauer spectra could be questionable because at nanometric scale the Mössbauer parameters are strongly influenced by dynamic and surface effects. The increase of saturation magnetization values σ_s in the 200–300 °C temperature range confirm the increase of the bulk spinel phase (Fig. 7).

Increasing the heating rate and the calcination temperature favor the conversion of spinel oxides in to α-Fe_2O_3. This behavior is well reflected by the Mössbauer spectra as well as by the saturation magnetization measurements.

4. Mechanism

For the decomposition of the $[Fe(urea)_6](NO_3)_3$ a mechanism can be proposed, which explains not only the generation of different volatile products but also the presence and the convertability of different iron hydroxide and iron oxide species (Fig. 8). After melting (2), a simultaneously release of nitrate urea and NO_2 take place ((3) and (4)). Subsequent, urea

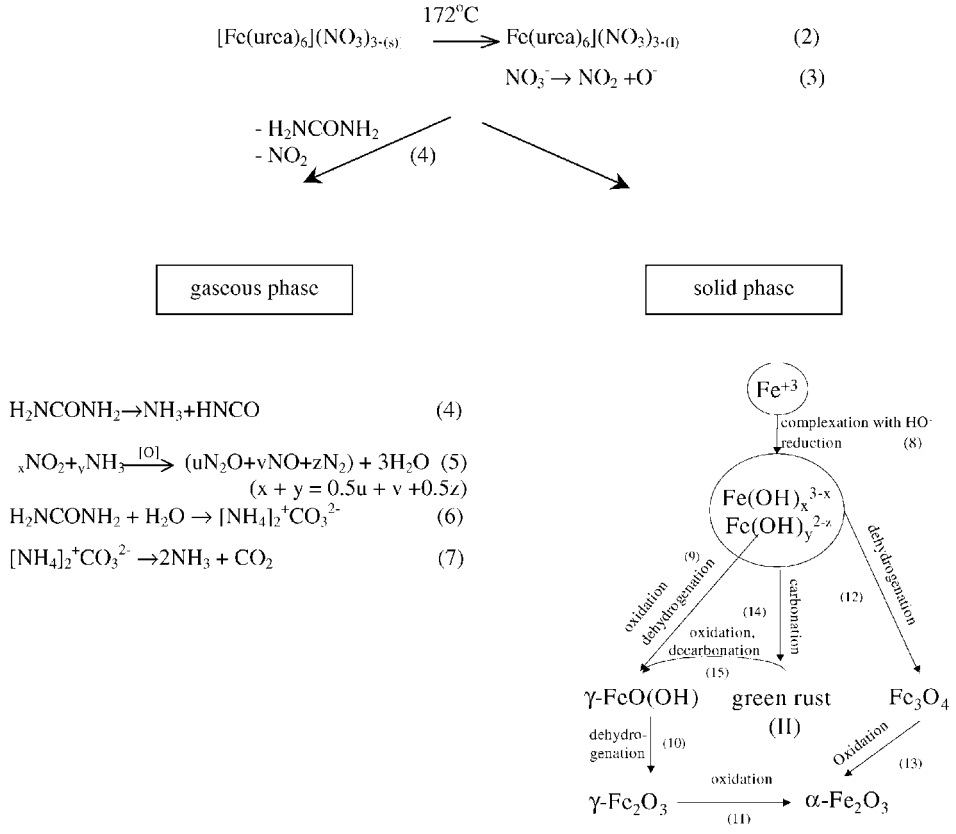

Fig. 8. Thermal decomposition mechanism.

conversion (4), and ammonia oxidation by NO_2 (5) occur. Due to the hydrolysis of the undecomposed urea, CO_2 may also be formed ((6) and (7)). On the other hand, the thermal decomposition product medium favors besides a partial reduction of iron ions, their coordination with HO^- (8). On heating, the complex intermediates are converted into different iron hydroxides and oxyhydroxides species, via successive oxidation and dehydrogenation processes ((9)–(13)). The presence of CO_2 and the oxygen deficit of the reaction medium promote the formation in a small extent, of green rust (II) (14), which further is converted into an oxyhydroxide (15).

Acknowledgements

O. Carp wishes to thank the German Academic Exchange Service for the fellowship. The authors also thank U. Sazama and N. Stanica for technical assistance.

References

[1] G. Bate, in: D.J. Craik (Ed.), Magnetic Oxides, Wiley, London, 1975, p. 697.
[2] A.K. Nikumba, K.S. Rane, A.J. Mukhadkhor, J. Mater. Sci. 18 (1983) 3415.
[3] T. Ishikawa, H. Nakazaki, A. Yasukawa, K. Kandori, M. Seto, Mater. Res. Bull. 11 (1998) 1609.
[4] S. Musič, M. Malij-Kovic, I. Czakó-Nagy, Mater. Lett. 31 (1997) 43.
[5] B.K. Das, in: J.M. Hönig, C.N.R. Rao (Eds.), Preparation and Characterization of Materials, Academic Press, New York, 1981, p. 75.
[6] R.C. Pullar, D.R. Pyke, M.D. Taylor, A.K. Bhattacharya, J. Mater. Sci. 33 (1980) 5229.
[7] D. Barb, L. Diamandescu, D. Mihaila-Tarabasanu, M. Morariu, A. Rusi, Hyp. Int. 53 (1990) 285.
[8] Y. Konishi, T. Kawamura, S. Asai, Ind. Eng. Chem. Res. 32 (1993) 2888.
[9] T. Dubois, G. Damazeau, Mater. Lett. 19 (1994) 38.
[10] L. Diamandescu, D. Mihaila-Tarabasanu, V. Teodorescu, N. Popescu-Pogrion, Mater. Lett. 6 (1998) 340.
[11] D. Chen, R. Xu, Mater. Res. Bull. 7 (1998) 1015.
[12] L. Diamandescu, D. Mihaila-Tarabasanu, N. Popescu-Pogrion, A. Totovina, I. Bibicu, Ceram. Int. 25 (1999) 689.
[13] R.A. Brown, S.C. Bevan, J. Inorg. Chem. 28 (1966) 382.
[14] R.C. Mackenzie, Differential Thermal Analysis, Vol. 1, Academic Press, New York, 1970, p. 274.
[15] J. Matutes-Aquino, P. Garcia-Casillas, O. Ayala-Valenzuela, S. Garcia-Garcia, Mater. Lett. 38 (1999) 173.
[16] R. Ravindranathan, R.C. Patil, Am. Ceram. Soc. Bull. 66 (1987) 688.
[17] L. Patron, O. Carp, I. Mindru, L. Petre, M. Brezeanu, Rev. Roum. Chim. 43 (1998) 173.
[18] A.I. Vogel, Quantitative Inorganic Analysis, 3rd Edition, Longman, London, 1961, p. 309.
[19] R.B. Penland, S. Mizushima, C. Curran, J.V. Quagliano, J. Am. Chem. Soc. 79 (1957) 1575.
[20] K. Nakamoto, Infrared Spectra of Inorganic and Coordination Compounds, 4th Edition, Wiley, New York, 1978, p. 268.
[21] M.S. Nelson, Comprehensive Coordination Chemistry, Vol. 4, Pergamon Press, Oxford, 1986, p. 217.
[22] R. Keuleers, J. Janssens, H.O. Desseyn, Thermochim. Acta 354 (2000) 125.
[23] R. Keuleers, G.S. Papaefstathiou, C.P. Raptopoulou, S.P. Perlepes, H.O. Desseyn, J. Mol. Struct. 525 (2000) 173.
[24] O.S. Josyulu, J. Sobhanadri, Phys. Stat. Sol. A 65 (1981) 479.
[25] P. Tarte, Spectrochim. Acta 19 (1963) 49.
[26] E. Kester, B. Gillot, P. Perriat, Ph. Dufour, C. Villette, Ph. Thailhades, A. Rousset, J. Solid State Chem. 126 (7–14) (1996) 7.
[27] F. Hochu, M. Lenglet, C.K. Jørgensen, J. Solid State Chem. 120 (1995) 244.